Gallery of Fluid Motion

Reconfiguring it out: How flexible structures interact with fluid flows

Mrudhula Baskaran, Louis Hutin, and Karen Mulleners*
Institute of Mechanical Engineering, École polytechnique fédérale de Lausanne (EPFL), Lausanne, Switzerland

(Received 3 June 2023; published 16 November 2023)

This paper is associated with a video winner of a 2022 American Physical Society's Division of Fluid Dynamics (DFD) Gallery of Fluid Motion Award for work presented at the DFD Gallery of Fluid Motion. The original video is available online at the Gallery of Fluid Motion, https://doi.org/10.1103/APS.DFD.2022.GFM.V0070

DOI: 10.1103/PhysRevFluids.8.110509

In nature, plants deform passively to withstand adverse weather conditions. The tall stems of sunflowers twist and reorient the flower to avoid directly facing incoming wind [Fig. 1(a)]. Tree leaves fold and wrap around themselves to streamline their shape and reduce the area exposed to the wind [Fig. 1(b)]. This passive process of streamlining and reducing the wind-facing area is referred to as reconfiguration and aids leaves in reducing their drag and staying attached to their branches, even during stormy weather [1,2]. Engineers want to mimic this flow-induced reconfiguration and deformation ability to design passive flexible valves [3,4], compact and stable parachutes [5,6], gust alleviation measures [7,8], etc. The practical design of these bio-inspired solutions requires an in-depth understanding of the unsteady interactions between the structural deformation of flexible structures facing the flow, the formation of vortices in the wake, and the drag experienced.

To systematically study the fluid-structure interaction of reconfiguring objects, we designed an experiment using thin disks of varying bending rigidity, which we translated vertically in quiescent water. The disks started from rest and were accelerated rapidly to reach a constant terminal velocity. We varied the terminal velocity, U, from 0.15 m/s to 0.5 m/s. This variation corresponds to a range of diameter-based Reynolds numbers from 9000 to 30 000. We tested disks of different thickness, h, to vary the bending rigidity, E. The disks had a diameter of 60 mm and thickness ranging from 25 μm to 175 μm. The thicker material has a higher bending rigidity. The bending rigidity of the materials were determined using an elastogravity bending test.

Depending on the bending rigidity of the disks and their translation velocity, the disks bend and reduce their projected area differently (Fig. 2). To allow the disks to bend in an axisymmetric way, we added radial cuts every 45°. We then overlapped two disks, offsetting the cuts, such that there was no flow through the cuts of the disks. During the translation, we measured the temporal evolution of the deformation of the disks along one radius using an optical setup with a laser sheet and camera, and the drag force on the disks using a load cell.

Example results are presented in Fig. 2. Once the disks start moving, they deform, until they reach an equilibrium state after a few disk diameters when the dynamic fluid pressure forces match the disk's bending restoring forces. Once this equilibrium state is reached, the diameter D of the

*karen.mulleners@epfl.ch

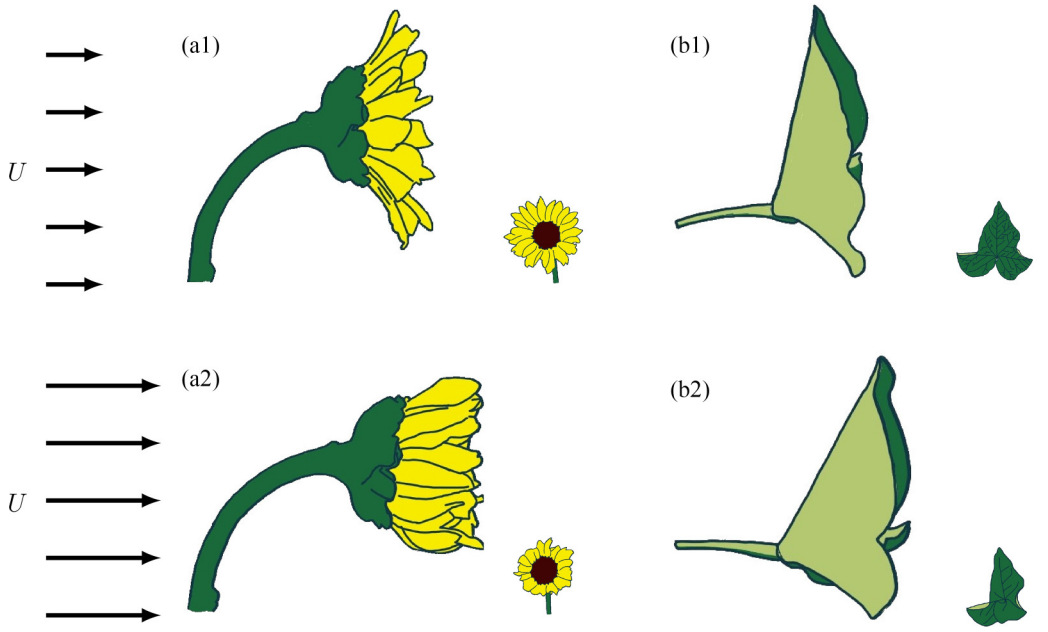

FIG. 1. Reconfiguration of a sunflower (a) and tree leaf (b) in response to low and high incoming wind speeds traced from photographs. The small insets show the view from the leeward side.

deformed disk remains constant until the motion is stopped. Minor fluctuations in the shape are associated to structural vibrations, and we focus here on the average diameter of the disk during the constant translation velocity phase. The dynamic behavior during the acceleration of the disk will be the topic of future work. The degree of deformation can be either increased by increasing the translational velocity [Figs. 2(a)–2(d)], or by decreasing the bending rigidity [Figs. 2(a), 2(e), 2(f), 2(g)]. The Cauchy number is defined as the ratio between the fluid forces and the bending rigidity of the disks: $Ca = (\rho U^2)/E$, where ρ is the density of water at 20 °C, 998 kg/m^3. The Cauchy number governs not only the deformation of the disks but also its steady state drag coefficient [9].

When the disks deform, they experience a lower drag force than rigid disks at the same velocity. The ratio of the drag force divided by the rigid disk drag is known in the literature as the reconfiguration number, $\mathscr{R} = D/D_{\text{rigid}}$ [11]. The evolution of the reconfiguration number with Cauchy number is presented in Fig. 2(h) for four disks with a different material thickness, h. For Cauchy numbers lower than unity, the disks behave like rigid disks. They barely deform, and the drag equals the rigid disk drag, yielding $\mathscr{R} = 1$. With increasing Cauchy number above unity, the disks deform increasingly and their relative drag decreases. The rate of decrease of the relative drag with Cauchy number is the same for all disks regardless of their thickness and is expressed by the Vogel exponent ($\mathscr{V}$) [10,12]. The Vogel exponent is determined as twice the slope of the reconfiguration number as a function of the Cauchy number in the log-log representation in Fig. 2(h). It indicates how the flow-induced drag deviates from a quadratic relationship. For rigid objects the drag increases with U^2. For reconfiguring objects, the drag increases with $U^{(2+\mathscr{V})}$. For all our disks, the Vogel exponent is approximately -0.80. The negative value of the Vogel exponent shows that the drag on deforming disks grows at a reduced rate compared to the drag on their rigid counterparts. The Vogel exponent illustrates how much the drag force deviates from scaling quadratically with the velocity. For the deforming disks, the drag approximately grows as $U^{2-0.8} = U^{1.2}$, highlighting the reduced drag growth rate compared to the rigid case.

Existing models that predict the drag on reconfigurable disks typically assume a uniform pressure distribution in the wake of the disk [9]. However, this pressure distribution is not uniform due to the

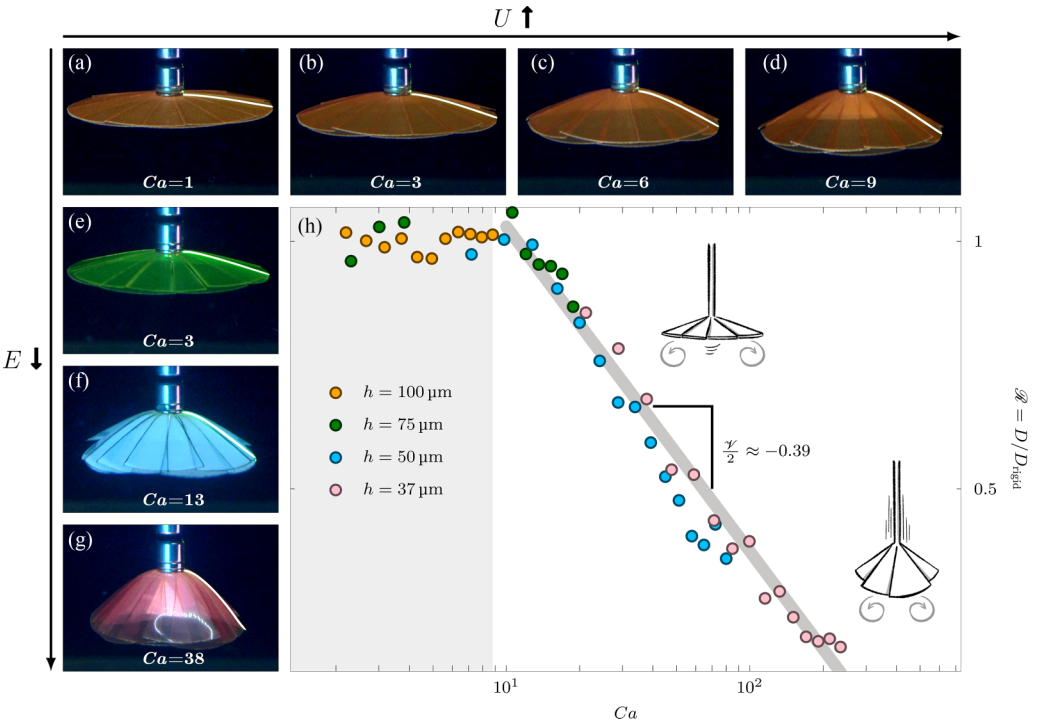

FIG. 2. Snapshots of the disks after they have reached an equilibrium deformation. The degree of deformation varies with the Cauchy number which was varied by varying the translational velocity of the disks, U (a)–(d), or the bending rigidity, E, by changing the thickness of the disk material, h, [(a), (e)–(g)]. Evolution of the reconfiguration number $\mathscr{R}$, defined as the ratio of the drag force, D, on the deformed disks and the drag on a rigid disk, D_{rigid}, at the same velocity (h). The slope of the evolution of the reconfiguration number as a function of the Cauchy number for $Ca > 1$ in the log-log plot is half of the Vogel exponent $\mathscr{V}$ [10]. For all disks, the Vogel exponent is approximately -0.8.

presence of an axisymmetric vortex ring below the disk [13]. The drag force mainly results from the difference in the pressure distribution upstream and downstream of the disk. A more accurate model for calculating the drag should include the temporal evolution of the vortex strength and size, which are directly linked to the disk's deformation. In future work, we plan to compute the vortex quantities from time-resolved velocity field measurements in the wake of the disks. The simple setup highlighted in our video can offer insights into how vortex-structure interactions influence the force and deformation of reconfigurable structures. This research can aid the design of robust and resilient flexible structures which harness vortex-structure interactions, such as drones and other aerial vehicles.

We acknowledge the Swiss National Science Foundation Grant No. 200021_175792 for funding this research. We thank Naïs Coq (nais.coq@gmail.com) for the sketches of the disks included in Fig. 2.

[1] E. de Langre, Effects of wind on plants, Annu. Rev. Fluid Mech. **40**, 141 (2008).
[2] F. P. Gosselin, Mechanics of a plant in fluid flow, J. Exp. Bot. **70**, 3533 (2019).

[3] K. Park, A. Tixier, A. H. Christensen, S. F. Arnbjerg-Nielsen, M. A. Zwieniecki, and K. H. Jensen, Viscous flow in a soft valve, J. Fluid Mech. **836**, R3 (2018).
[4] K. Park, A. Tixier, M. Paludan, E. Østergaard, M. Zwieniecki, and K. H. Jensen, Fluid-structure interactions enable passive flow control in real and biomimetic plants, Phys. Rev. Fluids **6**, 123102 (2021).
[5] H. G. Heinkich and T. R. Hertner, Flexibility as a model parachute performance parameter, J. Aircraft **8**, 704 (1971).
[6] H. Johari and K. J. Desabrais, Vortex shedding in the near wake of a parachute canopy, J. Fluid Mech. **536**, 185 (2005).
[7] T. Nakata, R. Noda, S. Kumagai, and H. Liu, A simulation-based study on longitudinal gust response of flexible flapping wings, Acta Mech. Sin. **34**, 1048 (2018).
[8] M. A. Badger, H. Wang, and R. Dudley, Avoiding topsy-turvy: How Anna's hummingbirds (*Calypte anna*) fly through upward gusts, J. Exp. Biol. **222**, jeb176263 (2019).
[9] F. Gosselin, E. de Langre, and B. A. Machado-Almeida, Drag reduction of flexible plates by reconfiguration, J. Fluid Mech. **650**, 319 (2010).
[10] T. Leclercq and E. de Langre, Drag reduction by elastic reconfiguration of non-uniform beams in non-uniform flows, J. Fluids Struct. **60**, 114 (2016).
[11] S. Alben, M. Shelley, and J. Zhang, Drag reduction through self-similar bending of a flexible body, Nature (London) **420**, 479 (2002).
[12] S. Vogel, *Life in Moving Fluids: The Physical Biology of Flow*, 2nd ed. (Princeton University Press, Princeton, NJ, 1994).
[13] G. de Guyon and K. Mulleners, Scaling of the translational velocity of vortex rings behind conical objects, Phys. Rev. Fluids **6**, 024701 (2021).